

## A catalog of white light coronal mass ejections observed by the SOHO spacecraft

S. Yashiro,<sup>1,2</sup> N. Gopalswamy,<sup>3</sup> G. Michalek,<sup>1,2,4</sup> O. C. St. Cyr,<sup>1,2</sup> S. P. Plunkett,<sup>5</sup> N. B. Rich,<sup>5</sup> and R. A. Howard<sup>5</sup>

Received 10 October 2003; revised 24 March 2004; accepted 29 April 2004; published 14 July 2004.

[1] The Solar and Heliospheric Observatory (SOHO) mission's white light coronagraphs have observed nearly 7000 coronal mass ejections (CMEs) between 1996 and 2002. We have documented the measured properties of all these CMEs in an online catalog. We describe this catalog and present a summary of the statistical properties of the CMEs. The primary measurements made on each CME are the apparent central position angle, the angular width in the sky plane, and the height (heliocentric distance) as a function of time. The height-time measurements are then fitted to first- and second-order polynomials to derive the average apparent speed and acceleration of the CMEs. The statistical properties of CMEs are (1) the average width of normal CMEs ( $20^\circ < \text{width} \leq 120^\circ$ ) increased from  $47^\circ$  (1996; solar minimum) to  $61^\circ$  (1999; early phase of solar maximum) and then decreased to  $53^\circ$  (2002; late phase of solar maximum), (2) CMEs were detected around the equatorial region during solar minimum, while during solar maximum CMEs appear at all latitudes, (3) the average apparent speed of CMEs increases from  $300 \text{ km s}^{-1}$  (solar minimum) to  $500 \text{ km s}^{-1}$  (solar maximum), (4) the average apparent speed of halo CMEs ( $957 \text{ km s}^{-1}$ ) is twice of that of normal CMEs ( $428 \text{ km s}^{-1}$ ), and (5) most of the slow CMEs ( $V \leq 250 \text{ km s}^{-1}$ ) show acceleration while most of the fast CMEs ( $V > 900 \text{ km s}^{-1}$ ) show deceleration. Solar cycle variation and statistical properties of CMEs are revealed with greater clarity in this study as compared with previous studies. Implications of our findings for CME models are discussed. *INDEX TERMS:* 7513 Solar Physics, Astrophysics, and Astronomy: Coronal mass ejections; 7536 Solar Physics, Astrophysics, and Astronomy: Solar activity cycle (2162); 7509 Solar Physics, Astrophysics, and Astronomy: Corona; 7599 Solar Physics, Astrophysics, and Astronomy: General or miscellaneous; *KEYWORDS:* Coronal Mass Ejections (CMEs)

**Citation:** Yashiro, S., N. Gopalswamy, G. Michalek, O. C. St. Cyr, S. P. Plunkett, N. B. Rich, and R. A. Howard (2004), A catalog of white light coronal mass ejections observed by the SOHO spacecraft, *J. Geophys. Res.*, 109, A07105, doi:10.1029/2003JA010282.

### 1. Introduction

[2] Although the concept of mass ejection from the Sun has been known for a long time, the phenomenon of coronal mass ejections (CMEs) as we know them today was first discovered in 1971 using the seventh Orbiting Solar Observatory (OSO-7) coronagraph [Tousey, 1973]. Several spaceborne coronagraphs such as the Apollo Telescope Mount (ATM) coronagraph [MacQueen et al., 1974] on board Skylab, the Solwind coronagraph [Michels et al., 1980] on board the P78-1 satellite, the Coronagraph/Polarimeter [MacQueen et al., 1980] on board the Solar Maximum Mission (SMM), and currently the Large Angle and

Spectrometric Coronagraph (LASCO) [Brueckner et al., 1995] on board the Solar and Heliospheric Observatory (SOHO) mission [Domingo et al., 1995] have observed CMEs. The Mauna Loa K-Coronameter is a ground-based instrument [Fisher et al., 1981] which has been observing CMEs close to the Sun for many years. These instruments had different characteristics and capabilities (see Howard et al. [1997], who compared the capabilities of various coronagraphs for detecting CMEs). The LASCO coronagraphs have helped us track CMEs up to a heliocentric distance of  $\sim 32 R_s$  for the first time.

[3] The OSO-7 coronagraph was able to record only 23 CMEs [Tousey et al., 1974] and Skylab observed 110 CMEs [Hildner et al., 1976; Gosling et al., 1976]. The number of CMEs observed in the next decade jumped by an order of magnitude, thanks to the SMM Coronagraph/Polarimeter and the Solwind coronagraph. Almost one solar cycle (1980–1989) was covered by combining Solwind and SMM observations, and over 2000 CMEs were detected. Data from these coronagraphs have been archived in catalogs [Howard et al., 1985; St. Cyr and Burkepile, 1990; Burkepile and St. Cyr, 1993], and statistical properties of locations, angular widths, and speeds of CMEs have been

<sup>1</sup>Catholic University of America, Washington, D.C., USA.

<sup>2</sup>Also at NASA Goddard Space Flight Center, Greenbelt, Maryland, USA.

<sup>3</sup>NASA Goddard Space Flight Center, Greenbelt, Maryland, USA.

<sup>4</sup>Also at Astronomical Observatory of Jagiellonian University, Krakow, Poland.

<sup>5</sup>Naval Research Laboratory, Washington, D.C., USA.

**Table 1.** Annual Variation of Coronal Mass Ejection (CME) Properties

Year	Number	$\phi$ , deg S, N <sup>a</sup>	Average (Median) Width, deg <sup>b</sup>	Average (Median) Speed, km/s
1996	204	-24, 20	47 (43)	281 (250)
1997	351	-17, 21	58 (55)	320 (271)
1998	697	-40, 40	56 (53)	421 (363)
1999	957	-56, 64	61 (58)	499 (440)
2000	1580	-61, 65	57 (52)	502 (447)
2001	1465	-58, 50	56 (52)	481 (410)
2002	1652	-59, 51	53 (49)	521 (468)

<sup>a</sup>Critical latitude: 80% of CMEs lie between 0° (equator) and  $\phi$  in apparent latitude.

<sup>b</sup>Average (median) angular width of CMEs whose width are between 20° and 120°.

studied (e.g., *Howard et al.* [1985], *Hundhausen* [1993], *Hundhausen et al.* [1994], *St. Cyr et al.* [1999], and *Kahler* [1992] for review). The SOHO/LASCO observations have already doubled the number of CMEs observed by the previous coronagraphs, exceeding 7000 by January 2003. A single instrument has never before observed this many CMEs, so this is a great opportunity to examine the statistical properties of CMEs again. Some of the properties of the SOHO/LASCO CMEs have been described by *Howard et al.* [1997], *St. Cyr et al.* [2000], and *Gopalswamy et al.* [2003a, 2003b, 2004]. In this paper we provide a complete description of the online catalog (section 2), which contains both the observed and derived properties of all the CMEs. In section 3 we describe the statistical properties of CMEs. In section 4 we compare our results with those of previous studies and discuss the implications of our findings for CME models. Finally, we summarize the results in section 5.

## 2. Online CME Catalog

### 2.1. CME Identification

[4] This catalog contains all the CMEs detected by the LASCO coronagraphs C2 and C3, which cover a combined field of view of 2.1 to 32  $R_s$ . The innermost coronagraph C1 operated only for the first 2.5 years; therefore we will not include C1 observations here. Both C2 and C3 have the same image size (1024 × 1024 pixels) with a pixel size of 11.2 and 56.0 arc sec, respectively. The starting point of our measurements is the data assembled in what is known as the movie (MVI) format. To reduce the file size, MVI data are compressed to half the resolution (512 × 512 pixels) before making the measurements. LASCO operators maintain a log, which contains notes (CME direction, flare association, data gap, and so on) on most of the CMEs observed daily. We use this log (available at <http://lasco-www.nrl.navy.mil/cmelist.html>) as a guide for our measurements. We also run movies of LASCO images and identify any missing CMEs. We use standard LASCO software available as Interactive Data Language (IDL) routines in solarsoft [*Freeland and Handy*, 1998] (available at <http://www.lmsal.com/solarsoft/>) to run movies of LASCO images and measure the increase in height of CMEs as they expand away from the Sun. We typically use the running difference movies to better identify frame-to-frame changes in the corona.

[5] When a new brightness enhancement (white light) moves outward in at least two consecutive LASCO images,

we define it as a CME. Even in a single LASCO image, if the shape of an enhancement is undoubtedly CME-like (e.g., the enhancement has typical CME three-part structure), we list it as a CME in the catalog. However, manual CME identification is subjective; different observers are likely to identify CMEs differently. The different CME identifications by different observers are discussed in section 4.1.

[6] A total of 6907 CMEs were observed from January 1996 to December 2002 as summarized in Table 1. The first column of Table 1 shows the number of CMEs in each calendar year. There were occasional data gaps when SOHO was not taking observations, including a huge data gap from June to October 1998 when SOHO was temporarily disabled. A detailed analysis of the SOHO/LASCO downtime and how it affects the estimate of CME production rate has been reported by *Gopalswamy et al.* [2003a, 2003b, 2004].

[7] The online CME catalog has been viewed and checked by the catalog team and users for more than 2 years, but we still occasionally find new CMEs. From the new information on the solar surface provided by X-ray and EUV observations, we could identify the new CMEs in the aftermaths of the previous CME. *St. Cyr et al.* [2000] noted from their experience with Solwind, SMM, and MLSO coronagraph data that any CME compilation must be viewed as living document. This statement applies to this catalog also. The catalog is unlikely to have major revision but will certainly have minor revisions.

### 2.2. CME Measurements and Basic Attributes

[8] The basic measurement is the height of the leading edge (LE) of CMEs, measured from the disk center (not from the solar limb). The height measurements are made at the position angle (PA) where the CME's LE moves fastest (PA is measured counterclockwise from Solar North in degrees). We call this PA the measurement PA (MPA). The measurements are made in each frame at which the CME's LE can be identified above the noise level. We also note the central position angle (CPA) defined as the mid-angle with respect to the two edges of the CME in the sky plane. All CMEs do not move symmetrically with respect to the CPA, so the MPA will differ slightly from the CPA. CMEs which appear to surround the occulting disk are marked as halo CMEs [*Howard et al.*, 1982]. Although we cannot define a CPA for the halo CMEs, we identify the MPA. Another basic attribute of a CME is its sky-plane width. This is twice the cone angle of the CME. The height-time plots are then fitted to first-order (constant speed) and second-order (constant acceleration) polynomials to characterize the motion of the CMEs. The first-order fit gives the average speed of the CME within the LASCO field of view. The second-order fit gives the average acceleration of the CME. The height-time profiles of CMEs fall into three categories: accelerating, constant speed, and decelerating [*Gopalswamy et al.*, 2001a]. The actual height-time measurements are also given in the catalog. Note that we can only measure the apparent CME properties projected in the sky plane. Therefore the real CME speed could be higher and angular width could be lower.

[9] The online catalog resides at [http://cdaw.gsfc.nasa.gov/CME\\_list/](http://cdaw.gsfc.nasa.gov/CME_list/). Figure 1a shows the general arrangement of the catalog as a matrix of years and months of observation. Figure 1b shows an actual entry in the catalog. Each CME is

**(a) SOHO LASCO CME CATALOG**

YEAR	MONTH											
1996	<a href="#">Jan</a>	<a href="#">Feb</a>	<a href="#">Mar</a>	<a href="#">Apr</a>	<a href="#">May</a>	<a href="#">Jun</a>	<a href="#">Jul</a>	<a href="#">Aug</a>	<a href="#">Sep</a>	<a href="#">Oct</a>	<a href="#">Nov</a>	<a href="#">Dec</a>
1997	<a href="#">Jan</a>	<a href="#">Feb</a>	<a href="#">Mar</a>	<a href="#">Apr</a>	<a href="#">May</a>	<a href="#">Jun</a>	<a href="#">Jul</a>	<a href="#">Aug</a>	<a href="#">Sep</a>	<a href="#">Oct</a>	<a href="#">Nov</a>	<a href="#">Dec</a>
1998	<a href="#">Jan</a>	<a href="#">Feb</a>	<a href="#">Mar</a>	<a href="#">Apr</a>	<a href="#">May</a>	<a href="#">Jun</a>	<a href="#">Jul</a>	<a href="#">Aug</a>	<a href="#">Sep</a>	<a href="#">Oct</a>	<a href="#">Nov</a>	<a href="#">Dec</a>
1999	<a href="#">Jan</a>	<a href="#">Feb</a>	<a href="#">Mar</a>	<a href="#">Apr</a>	<a href="#">May</a>	<a href="#">Jun</a>	<a href="#">Jul</a>	<a href="#">Aug</a>	<a href="#">Sep</a>	<a href="#">Oct</a>	<a href="#">Nov</a>	<a href="#">Dec</a>
2000	<a href="#">Jan</a>	<a href="#">Feb</a>	<a href="#">Mar</a>	<a href="#">Apr</a>	<a href="#">May</a>	<a href="#">Jun</a>	<a href="#">Jul</a>	<a href="#">Aug</a>	<a href="#">Sep</a>	<a href="#">Oct</a>	<a href="#">Nov</a>	<a href="#">Dec</a>
2001	<a href="#">Jan</a>	<a href="#">Feb</a>	<a href="#">Mar</a>	<a href="#">Apr</a>	<a href="#">May</a>	<a href="#">Jun</a>	<a href="#">Jul</a>	<a href="#">Aug</a>	<a href="#">Sep</a>	<a href="#">Oct</a>	<a href="#">Nov</a>	<a href="#">Dec</a>
2002	<a href="#">Jan</a>	<a href="#">Feb</a>	<a href="#">Mar</a>	<a href="#">Apr</a>	<a href="#">May</a>	<a href="#">Jun</a>	<a href="#">Jul</a>	<a href="#">Aug</a>	<a href="#">Sep</a>	<a href="#">Oct</a>	<a href="#">Nov</a>	<a href="#">Dec</a>

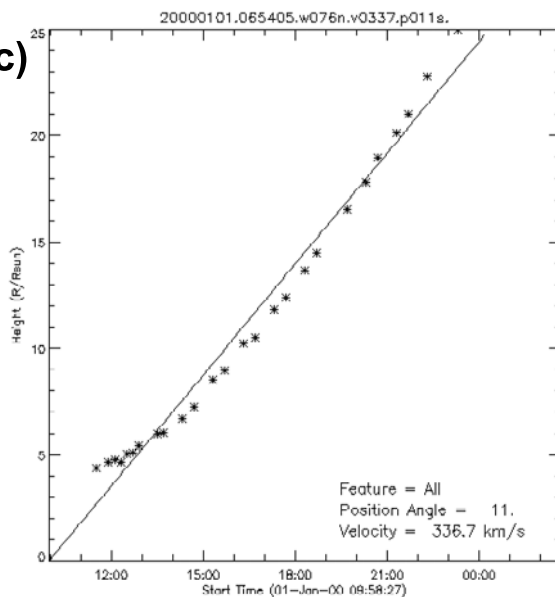
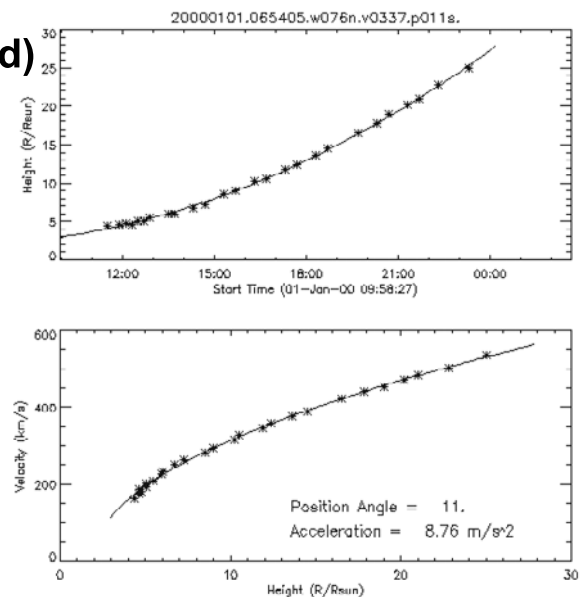
Click on month to get the list of CMEs for that month

[Publications using SOHO/LASCO CME Catalog](#)

[Text only version](#)

**(b)**

First C2 Appearance Date Time [UT]	Central PA [deg]	Angular Width [deg]	Linear fit Speed [km/s]	2nd order fit Speed [km/s]		Accel [m/s <sup>2</sup> ]	Measurement PA [deg]	Daily Movies and Daily Plots	Remark
<a href="#">2000/01/01 06:54:05</a>	21	76	<a href="#">337</a>	<a href="#">531</a>	<a href="#">470</a>	8.8	11	<a href="#">C2 C3 195</a> <a href="#">SXT PHTX</a> <a href="#">Java Movie</a>	
<a href="#">2000/01/01 14:30:05</a>	226	62	<a href="#">506</a>	<a href="#">614</a>	<a href="#">563</a>	6.3	228	<a href="#">C2 C3 195</a> <a href="#">SXT PHTX</a> <a href="#">Java Movie</a>	
<a href="#">2000/01/01 14:30:05</a>	77	106	<a href="#">196</a>	<a href="#">319</a>	<a href="#">362</a>	5.0	88	<a href="#">C2 C3 195</a> <a href="#">SXT PHTX</a> <a href="#">Java Movie</a>	
<a href="#">2000/01/02 01:31:18</a>	167	27	<a href="#">385</a>	<a href="#">476</a>	<a href="#">512</a>	7.2	171	<a href="#">C2 C3 195</a> <a href="#">SXT PHTX</a> <a href="#">Java Movie</a>	

**(c)****(d)**

**Figure 1.** (a) Overview of online catalog as a matrix of years and months of observation. (b) A few of the entries in the catalog for 1–2 January 2000. (c–d) Height-time plots in the catalog obtained by linear (left) and for quadratic (right) fits to the measurements (asterisks). See color version of this figure in the HTML.

identified by the date and time of occurrence. The catalog contains a number of attributes that characterize the CMEs: date and time of first appearance in the C2 coronagraph field of view, CPA, angular width, speed from linear fit to the height-time measurements, speed from quadratic fit at the last height of measurement, speed from quadratic fit at  $20 R_s$ , acceleration obtained from the quadratic fit, and MPA. By clicking on the date, one can view javascript movies of the CMEs within the C2 field of view, with the 195 Å images from the extreme ultraviolet imaging telescope (EIT) [Delaboudiniere *et al.*, 1995] superimposed so that the solar source of the CMEs could potentially be identified. By clicking on the time, one can view the actual height-time measurements. By clicking on the linear or second-order speeds, one can view the height-time plots with linear and quadratic fits (in png format; see Figures 1c and 1d). Links are also provided to the LASCO and EIT daily movies created at the Naval Research Laboratory.

### 3. CME Properties

#### 3.1. Apparent Width

[10] In order to determine the apparent angular width and CPA of the CMEs, we measure the PA of the two outer edges of CMEs in the sky plane. The PA extents are generally measured using C2 data. If C2 data are not available, C3 data are used. If the apparent width gradually increases with time, we measure the PA when the width reaches maximum. The difference between the edge PAs is taken as the apparent width of the CMEs; the CPA is defined as the midangle between the edge PAs. CMEs which appear to surround the occulting disk [Howard *et al.*, 1982] are labeled “halo.” Gopalswamy *et al.* [2003b] classified the halo CMEs as type F (full halos), type A (asymmetric halos), and type P (partial halos). F halos generally originate from close to the disk center or from behind the limb. Type A halos are wide, close to limb CMEs in the C2 field of view, but by the time they expand to C3 field of view, they have a faint extension above the opposite limb [Sheeley *et al.*, 2000]. In this catalog, type F and type A halos are labeled “halo.” Type P halos are CMEs with width greater than  $120^\circ$ , but they never completely surround the occulting disk within the LASCO field of view.

[11] Figure 2 shows distributions of the apparent angular width ( $W$ ) from January 1996 through December 2002. The last bins with widths greater than  $180^\circ$  include halo CMEs. The observed number of CMEs in each year is shown on the plots. During solar minimum (1996–1997), the shape of the distributions is simple with a peak at  $W \sim 40^\circ$ . During early solar maximum (1999–2000), the distribution has two peaks at  $15^\circ$  and  $50^\circ$ . The bimodal distribution disappears after 2001. The distributions become simple with a peak of  $\sim 20^\circ$ – $35^\circ$  during 2001–2002.

[12] In order to investigate the properties of CMEs with different angular widths, we simply grouped CMEs into three populations: narrow ( $W \leq 20^\circ$ ), normal ( $20^\circ < W \leq 120^\circ$ ), and wide ( $W > 120^\circ$ ) CMEs (From the bimodal distribution during early solar maximum, we can discern a population of narrow CMEs with  $W \leq 20^\circ$ . The CMEs with  $W > 120^\circ$  are called partial halos). The numbers and fractions of narrow, normal, and wide CMEs in each year are shown in Table 2. We found that the fraction of narrow CMEs increases toward

solar maximum. We note here that it may not be possible to identify all the narrow CMEs. If narrow CMEs occur in the aftermaths of wide CMEs, they will be missed since it is hard to distinguish the narrow CMEs and aftermaths (legs) of the wide CMEs. Therefore the numbers and fractions of narrow CMEs during solar maximum could be higher than observed. In fact, the annual number of narrow CMEs in 2001 is significantly less than in 2000 and 2002, while the number of wide CMEs is slightly higher.

[13] The width distribution of normal CMEs has a peak at  $W = 35^\circ$  in 1996. The peak shifted to  $50^\circ$  in 1999 and decreased to  $40^\circ$  in 2001. To estimate the typical width of CMEs properly, we used normal CMEs only. The average (median)  $W$  increased from  $47^\circ$  ( $43^\circ$ ) in 1996 to  $61^\circ$  ( $58^\circ$ ) in 1999 and then gradually decreased to  $53^\circ$  ( $49^\circ$ ) in 2002 (see Table 1). It is interesting that the average  $W$  of normal CMEs peaked during the early part of the solar maximum.

[14] The error in the average width ( $\bar{\sigma}_W$ ) can be derived from the propagation of errors of individual CME widths

$$(\sigma_W): \bar{\sigma}_W^2 = \frac{1}{n^2} \sum_{i=1}^n \sigma_{W_i}^2, \text{ where } n \text{ is total number of CMEs. If}$$

we assume that the error of angular width for each CME is 30% (50%), the error of average width becomes  $1.2^\circ$  ( $2.0^\circ$ ) for 1996 and  $0.6^\circ$  ( $0.9^\circ$ ) for 2000. The assumed large measurement errors are unlikely, but we see that the error of average width is very small because of the large number of CMEs measured. Therefore the solar cycle variation of the average and median CME widths is significant.

#### 3.2. Apparent Latitudes of CMEs

[15] In order to study the latitudes of CMEs, we converted CPAs to projected heliographic latitudes. For example, CPAs of  $0^\circ$ ,  $90^\circ$ ,  $180^\circ$ , and  $270^\circ$  correspond to the apparent latitudes of  $90^\circ$ ,  $0^\circ$ ,  $-90^\circ$ , and  $0^\circ$ , respectively. Figure 3 shows the distributions of apparent latitude of CMEs from 1996 through 2002. Halo CMEs are excluded since the CPAs cannot be determined for halo CMEs. During solar minimum (1996–1997), almost all CMEs occurred around the equator (within  $\pm 20^\circ$ ). This result is consistent with the distribution of the location of the streamer belt. In 1998, the distribution became wider ( $\pm 60^\circ$ ). During solar maximum (1999–2000), CMEs appeared at every latitude. This is in agreement with the results from Solwind [Howard *et al.*, 1985] and SMM [Hundhausen *et al.*, 1984; Hundhausen, 1993].

[16] Gopalswamy *et al.* [2003a, 2003c] examined the latitudes of CMEs associated with prominence eruptions and found a north-south asymmetry in the high-latitude activities. We confirm this result using the general population of LASCO CMEs. The vertical lines in Figure 3 show the critical latitude  $\phi$  (deg) defined as the latitude within which 80% of the CMEs lie. The third column in Table 1 also shows the annual variation of  $\phi$ . The CME activity at high latitudes in the north peaked during 1999–2000, while that in the south peaked during 2000–2002. Clear north-south asymmetry was shown in 2001–2002.

[17] Figure 4 shows the scatterplots of the apparent latitudes and widths for all CMEs (Figure 4a) and for normal CMEs (Figure 4b). Full and asymmetric halo CMEs are excluded again. The median widths in  $10^\circ$  latitude intervals are indicated by gray solid lines.

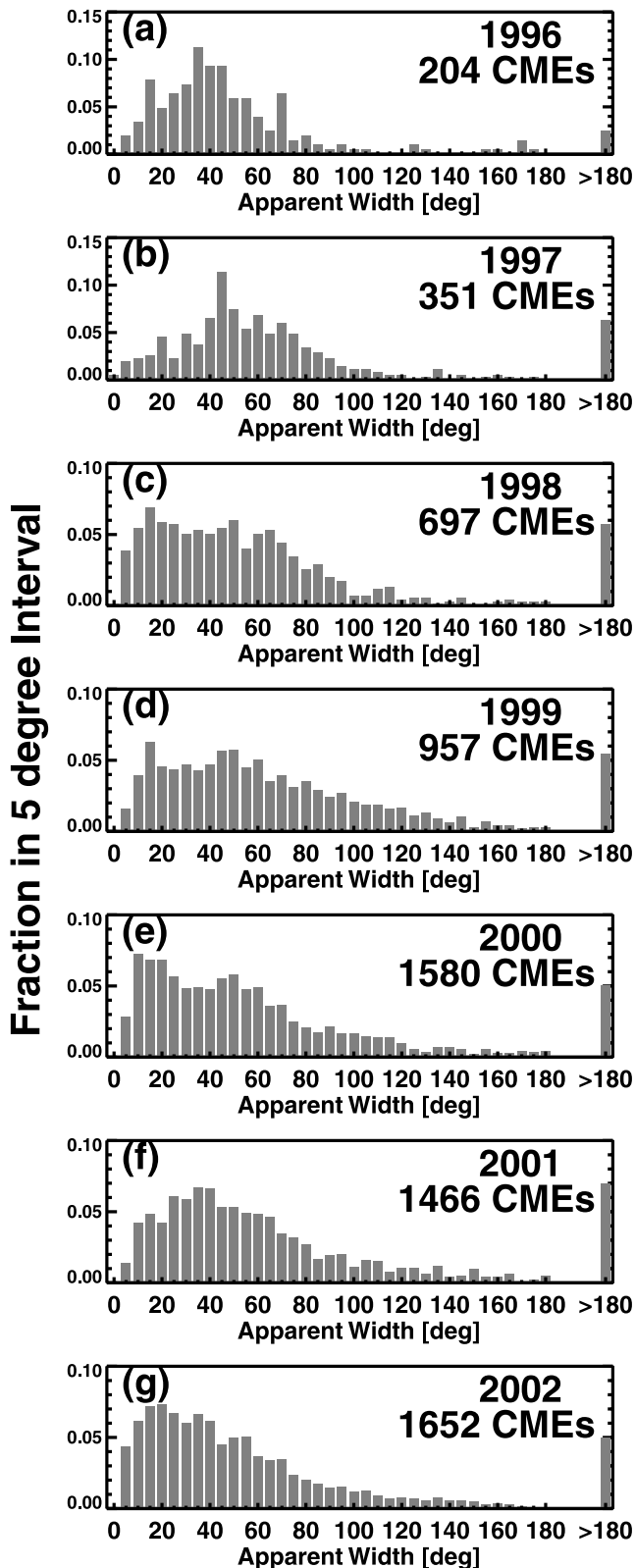


**Figure 2.** Distribution of apparent widths of coronal mass ejections (CMEs) from 1996 to 2002. The fractions in 5 degree interval are obtained by dividing the number of CMEs in each bin by the total number of CMEs. The year and number of CMEs obtained during that year are marked in each panel. Because of large data gaps, the number of CMEs listed needs to be treated as a lower limit.

The median widths of CMEs from high latitudes ( $>80^\circ$ ) are slightly larger than those from middle and low latitudes. A similar result was reported from the SMM data by *Hundhausen et al.* [1994], who mentioned that this may be due to projection effects (see also *Hundhausen* [1993]). We conclude that there is no clear relation between the apparent latitudes and widths.

### 3.3. Apparent Speeds of CMEs

[18] The CME speed is determined when at least two height measurements are available. We were able to measure the speeds of 6599 CMEs out of the 6907 detected. An insufficient number of data points or data gaps resulted in our inability to measure the speeds of about 4% of the CMEs. In order to measure the CME speeds properly, we need to track the same CME feature (leading edge) in each frame. However, it is difficult to track the same leading edge for the faint CMEs. Our ability depends on the clarity and sharpness of the leading edges. In order to rate the accuracy of the speed measurement, we define a quality index for the tracking feature of each CME: poor, fair, typical, good, and excellent. The quality indices are recorded in height-time digital files, as a numerical value between 1 (poor) and 5 (excellent). For a CME with an ill-defined leading edge we assign a quality index of zero.

[19] Figure 5 shows the apparent speed distributions for each calendar year with the average (annual) speeds. We use speeds from linear fits to height-time measurements even if the quadratic fit is more suitable. The average (median) speed increases toward solar maximum from  $300 \text{ km s}^{-1}$  ( $250 \text{ km s}^{-1}$ ) to  $500 \text{ km s}^{-1}$  ( $450 \text{ km s}^{-1}$ ) (see Table 1). The peak of the distribution also shifted from  $250 \text{ km s}^{-1}$  to  $400 \text{ km s}^{-1}$ . Table 3 shows the average and median speeds for narrow ( $W \leq 20^\circ$ ), normal ( $20^\circ < W \leq 120^\circ$ ), and wide ( $W > 120^\circ$ ) CMEs. During solar maximum the average (median) speed of normal CMEs ranged from  $452 \text{ km s}^{-1}$  to  $468 \text{ km s}^{-1}$  ( $405 \text{ km s}^{-1}$  to  $420 \text{ km s}^{-1}$ ) except for 2001. The average (median) speed of normal CMEs in 2001 was  $423 \text{ km s}^{-1}$  ( $372 \text{ km s}^{-1}$ ), significantly lower than in 2000 and 2002. The total number of CMEs in 2001 also showed this peculiarity (see Table 1). Table 3 also shows that the average speed of narrow CMEs peaked in 1999, while that of wide CMEs peaked in 2002.

#### 3.3.1. CME Speed and Angular Width

[20] Figure 6 shows the linear and logarithmic scatterplots between apparent speed and apparent angular width of the 6599 CMEs. The average speeds are shown by the solid lines in Figure 6. We calculated the average speeds in  $10^\circ$  bins for CMEs with  $W \leq 140^\circ$ . Since we do not have many CMEs

**Table 2.** Annual Numbers of Narrow, Normal, and Wide CMEs

Year	All	Narrow	Normal	Wide
1996	204	32 (16%)	158 (77%)	14 (6%)
1997	351	39 (11%)	277 (79%)	35 (9%)
1998	697	141 (20%)	489 (70%)	67 (9%)
1999	957	141 (15%)	683 (71%)	133 (13%)
2000	1580	330 (21%)	1077 (68%)	173 (10%)
2001	1465	193 (13%)	1063 (73%)	209 (14%)
2002	1652	376 (23%)	1110 (67%)	166 (10%)

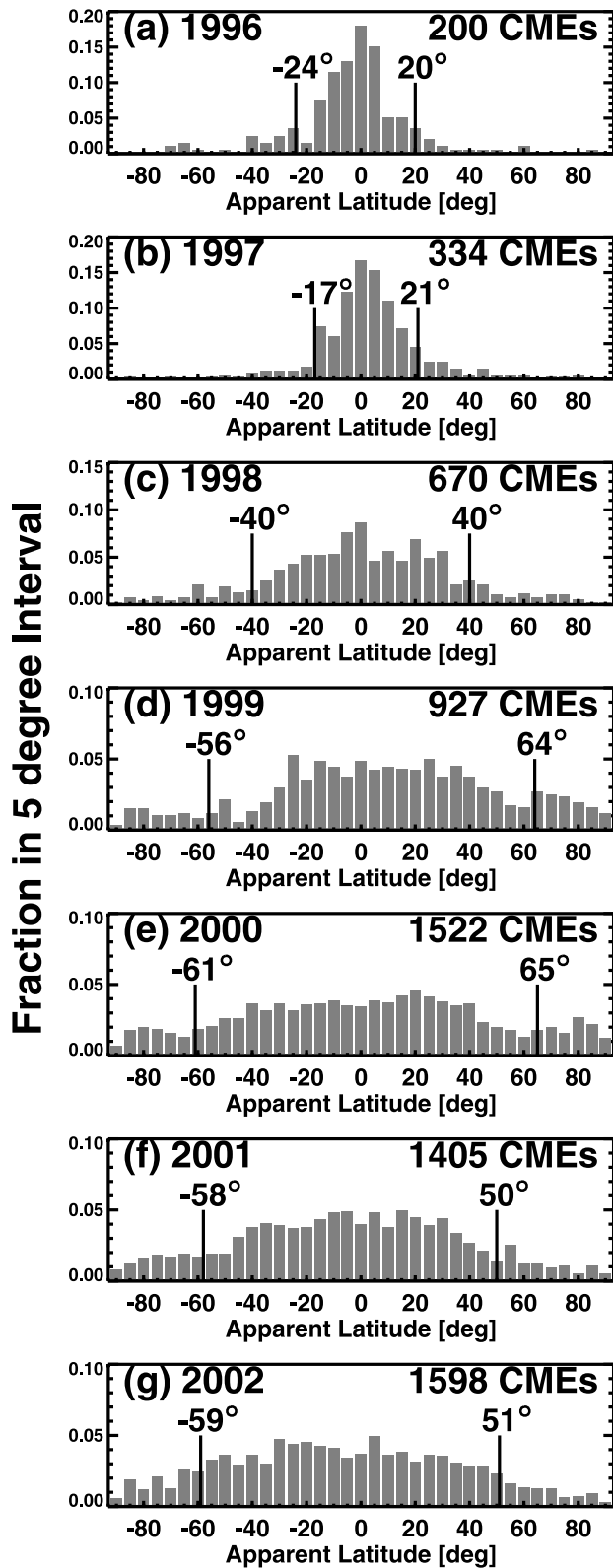


**Figure 3.** Distribution of apparent latitudes of CMEs from 1996 to 2002. The fractions in 5 degree interval are obtained by dividing the number of CMEs in each bin by the total number of CMEs.  $90^\circ$ ,  $0^\circ$ , and  $-90^\circ$  correspond to North Pole, equator, and South Pole, respectively. Halo CMEs are excluded.

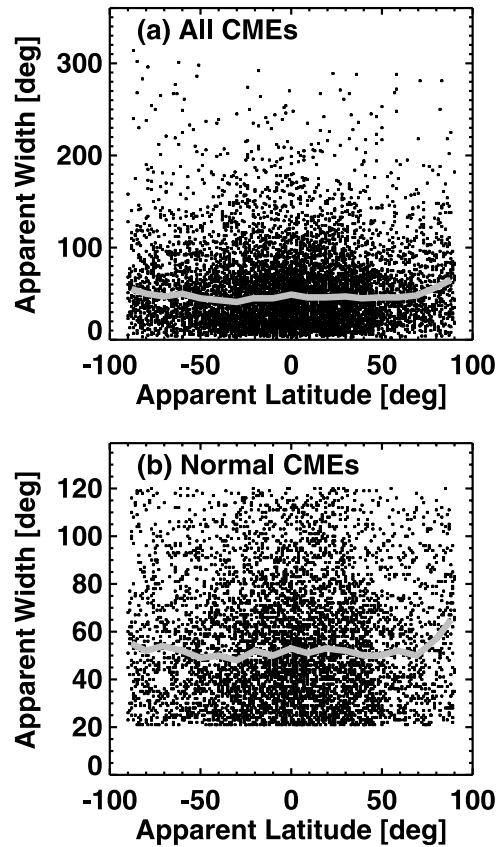


**Figure 4.** Scatterplots of CME width and latitude (a) for all CMEs and (b) for normal CMEs. Solid lines show the median width of CMEs in  $10^\circ$  latitude bins.

with  $W > 140^\circ$ , we changed the bin size to  $20^\circ$ ,  $160^\circ$ , and  $1^\circ$  for the CMEs with  $140^\circ < W \leq 200^\circ$ ,  $200^\circ < W < 360^\circ$ , and  $W = 360^\circ$ , respectively. For CMEs with  $W < 60^\circ$ , the average speed slightly decreased from  $508 \text{ km s}^{-1}$  ( $W = 0^\circ$  to  $10^\circ$ ) to  $398 \text{ km s}^{-1}$  ( $W = 60^\circ$  to  $70^\circ$ ). For CMEs with  $W > 60^\circ$ , a weak correlation between CME width and speed can be seen in Figure 6b. The average speed clearly increased with CME width from  $398 \text{ km s}^{-1}$  ( $W = 60^\circ$  to  $70^\circ$ ) to  $957 \text{ km s}^{-1}$  ( $W = 360^\circ$ ), even though the scatter is large. The correlation between CME width and speed was reported for SMM CMEs [Hundhausen *et al.*, 1994].

[21] In Figure 6b we also see that there are no slow ( $V < 100 \text{ km s}^{-1}$ ) and narrow ( $W < 10^\circ$ ) CMEs, and no slow ( $V < 100 \text{ km s}^{-1}$ ) and wide ( $W > 120^\circ$ ) CMEs. The upper boundary of the scatterplot in Figure 6b is not flat; wider CMEs tend to have higher speed. There were 16 CMEs with speeds more than  $2000 \text{ km s}^{-1}$ , and the fastest CME with a speed of  $2604 \text{ km s}^{-1}$  occurred on 12 May 2000. The minimum width of the very fast CMEs ( $V > 2000 \text{ km s}^{-1}$ ) was  $150^\circ$  (for the CME on 4 June 1999). Figure 6c is the scatterplot of CME speed and width for fast CMEs ( $V > 900 \text{ km s}^{-1}$ ). One can see that the width of the fast CMEs ranged from  $10^\circ$  to  $360^\circ$ , but there is also a weak correlation (correlation coefficient  $R = 0.44$ ). Similar correlation ( $r = 0.44$ ) was reported earlier for CMEs associated with decameter-hectometric (DH) radio bursts [Gopalswamy *et al.*, 2001a]. They also reported that the correlation for limb DH CMEs ( $r = 0.56$ ) is better than that of all DH

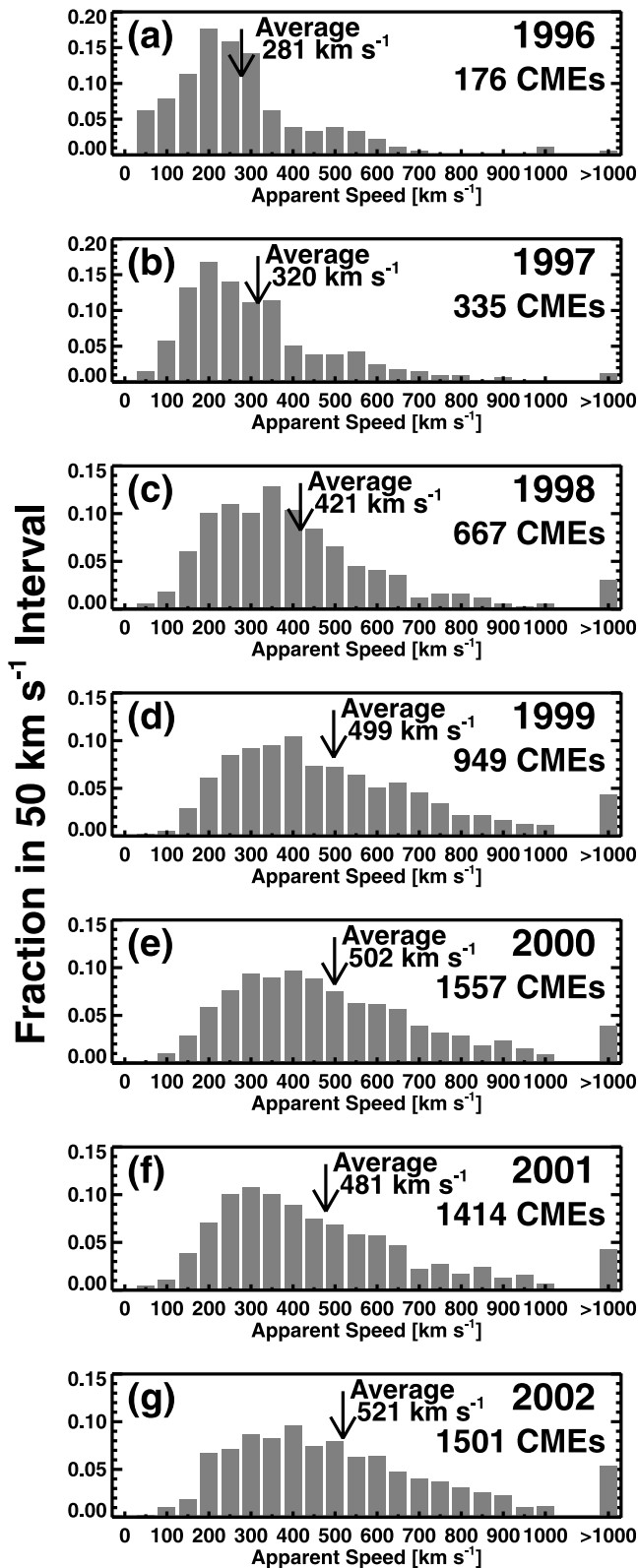


**Figure 5.** Apparent speed distribution of CMEs from 1996 through 2002. The fractions in  $50 \text{ km s}^{-1}$  interval are obtained by dividing the number of CMEs in each bin by the total number of CMEs. The average values of the distribution are marked by arrows in each panel.

CMEs ( $r = 0.44$ ) because there are minimal projection effects for the limb events.

### 3.4. Apparent Acceleration of CMEs

[22] If we have three or more height-time measurements, it is possible to determine the acceleration of CMEs. Quadratic fits to the height-time plots give the average acceleration within the LASCO field of view (FOV). We have listed all available accelerations even if linear fits are more suitable and/or errors of acceleration seem to be large. From the fit parameters we also obtain the speed at the first measurement point (initial speed) and at the last measurement point (final speed). These parameters are also listed in the online CME catalog (initial speeds are available only in the text-only version).

[23] The acceleration values are more difficult to obtain than the speeds. The error depends on the accuracy of each measurement and the number of measurement points. To illustrate this, we compared the errors in the derived speed ( $V$ ) and acceleration ( $a$ ) for three and five measurement points. We considered a CME at heights ( $R_s$ ) = [3, 4.5, 6] at times (min) = [0, 30, 60], respectively (crosses in Figure 7a). The time cadence of LASCO images is typically 30 min. Using linear and quadratic fits, we obtained  $V = 582 \text{ km s}^{-1}$  and acceleration  $a = 0$ . If the last measurement point shifts by  $0.1 R_s$  outward (inward), then the heights ( $R_s$ ) = [3, 4.5, 6.1 (5.9)] so that we obtain new values  $V_{\text{out}} = 601 \text{ km s}^{-1}$  ( $V_{\text{in}} = 562 \text{ km s}^{-1}$ ) and  $a_{\text{out}} = +22 \text{ m s}^{-2}$  ( $a_{\text{in}} = -22 \text{ m s}^{-2}$ ). The error in  $V$  is only  $\sim 4\%$ , but the error in  $a$  is significantly large. Figure 7b shows the errors in speed and acceleration for five measurement points. We considered the same CME at heights ( $R_s$ ) = [3, 4.5, 6, 7.5, 9] at times (min) = [0, 30, 60, 90, 120]. The fitted values are  $V = 582 \text{ km s}^{-1}$  and  $a = 0$ . If the last two measurement points shift by  $0.1 R_s$  outward (inward), then the heights equal [3, 4.5, 6, 7.6 (7.4), 9.1 (8.9)] so that we get  $V_{\text{out}} = 593 \text{ km s}^{-1}$  ( $V_{\text{in}} = 570 \text{ km s}^{-1}$ ) and  $a_{\text{out}} = +3 \text{ m s}^{-2}$  ( $a_{\text{in}} = -3 \text{ m s}^{-2}$ ). The error in acceleration is significantly smaller than the three-point measurement case.

[24] In this paper we required that the CME height measurements have at least five points to reduce the error in acceleration. CMEs with poorly defined leading edges (quality indices of CMEs are poor and fair; see section 3.3) were dropped because they result in large errors in the derived acceleration. Thus we were able to obtain accelerations for 3058 CMEs out of the 6907 detected. Figure 8 shows the relationship between the acceleration and speed for different speed ranges ( $V \leq 250 \text{ km s}^{-1}$ ,  $250 < V \leq 450 \text{ km s}^{-1}$ ,  $450 < V \leq 900 \text{ km s}^{-1}$ , and  $V > 900 \text{ km s}^{-1}$ ). Most of the slow CMEs seem to accelerate (Figure 8a). The peak of the distribution is at  $\sim 5 \text{ m s}^{-2}$ . Very few slow CMEs show deceleration. The speed profiles of the slow

**Table 3.** Average (Median) CME Speed in km/s

Year	Total	Narrow	Normal	Wide
1996	281 (250)	272 (255)	265 (240)	467 (480)
1997	320 (271)	323 (245)	304 (263)	437 (371)
1998	421 (363)	392 (372)	380 (349)	783 (619)
1999	499 (440)	578 (551)	454 (405)	649 (558)
2000	502 (447)	532 (508)	452 (408)	751 (702)
2001	481 (410)	488 (467)	423 (372)	762 (633)
2002	521 (468)	513 (479)	468 (420)	873 (829)

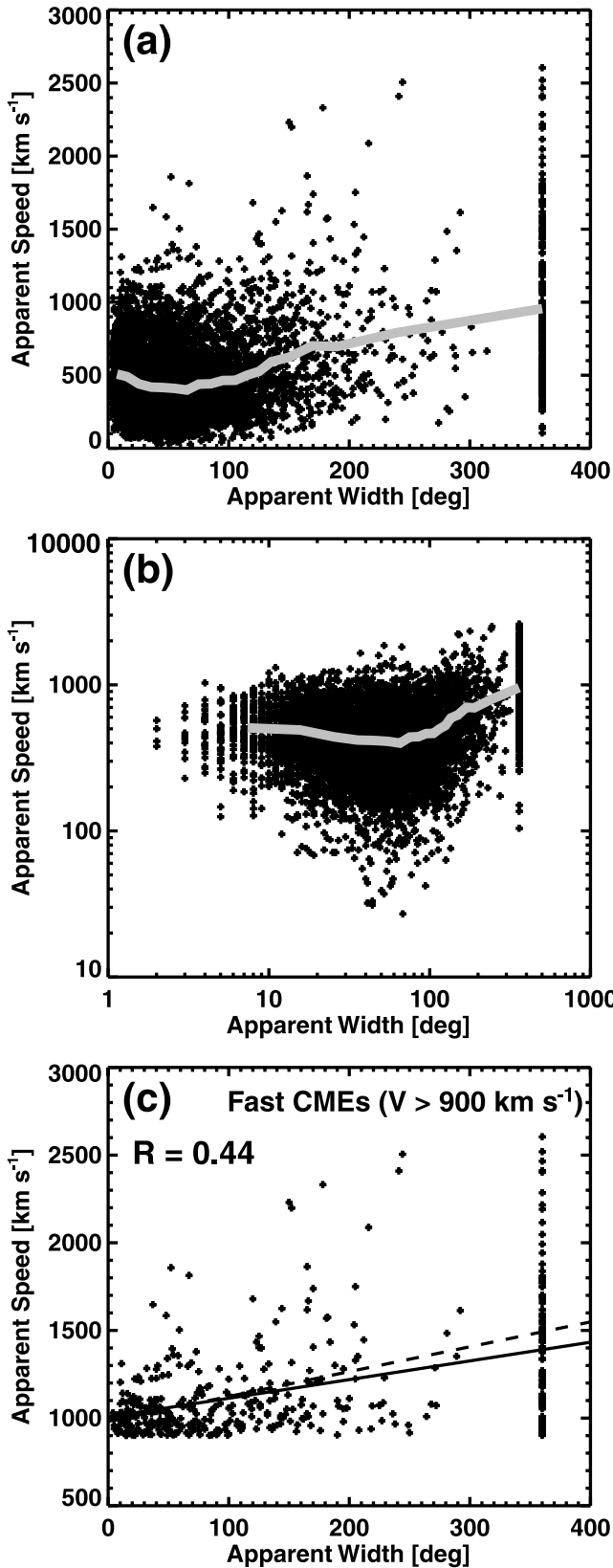


**Figure 6.** Scatterplots of CME width and speed in (a) linear and (b) logarithmic scales. Gray solid lines show the average CME speed. (c) Scatterplots of CME width and speed for fast ( $V \geq 900 \text{ km s}^{-1}$ ) CMEs.

CMEs and their average acceleration resemble those of the slow solar wind as was shown by *Sheeley et al.* [1997]. However, the measured speeds are apparent speeds, so the real speeds are possibly higher. For intermediate speeds ( $250 < V \leq 450 \text{ km s}^{-1}$ ), there is an equal number of accelerating and decelerating CMEs (Figure 8b). For fast CMEs ( $V > 450 \text{ km s}^{-1}$ ), there are more decelerating CMEs than accelerating ones (Figures 8c and 8d). The peaks are at  $\sim -5 \text{ m s}^{-2}$  and  $-15 \text{ m s}^{-2}$  for the distributions in Figures 8c and 8d, respectively. The decelerations are the largest for the fastest CMEs (Figure 8d). We found that most of the slow CMEs ( $V \leq 250 \text{ km s}^{-1}$ ) show acceleration, while most of fast CMEs ( $V > 900 \text{ km s}^{-1}$ ) show deceleration. An implication of these results is discussed in section 4.2.

## 4. Discussion

### 4.1. Number of CMEs

[25] The CME identification is carried out manually, so different observers are likely to see different number of CMEs. *St. Cyr et al.* [2000] identified, measured, and listed 841 LASCO CMEs from January 1996 to June 1998. However we identified 1083 CMEs during the same period. We carefully checked the difference of these two catalogs

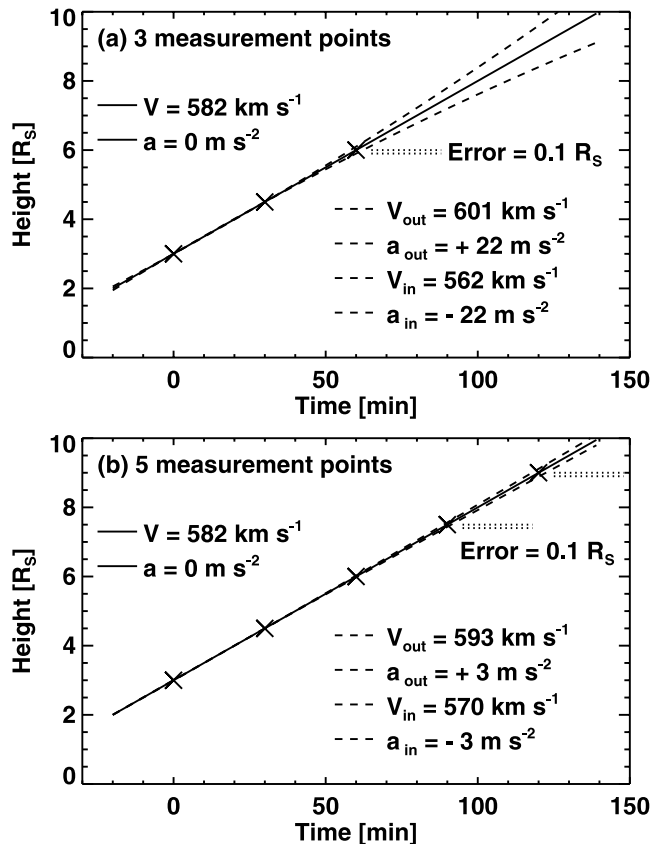


**Figure 7.** Errors in speed and acceleration measurements for (a) three data points and (b) five data points.  $V$  and  $a$  are the derived speed and acceleration for a set of height-time data points.  $V_{\text{out}}$  ( $V_{\text{in}}$ ) and  $a_{\text{out}}$  ( $a_{\text{in}}$ ) are the speeds and accelerations when the last height-time measurement is shifted by  $0.1 R_s$  outward (inward).

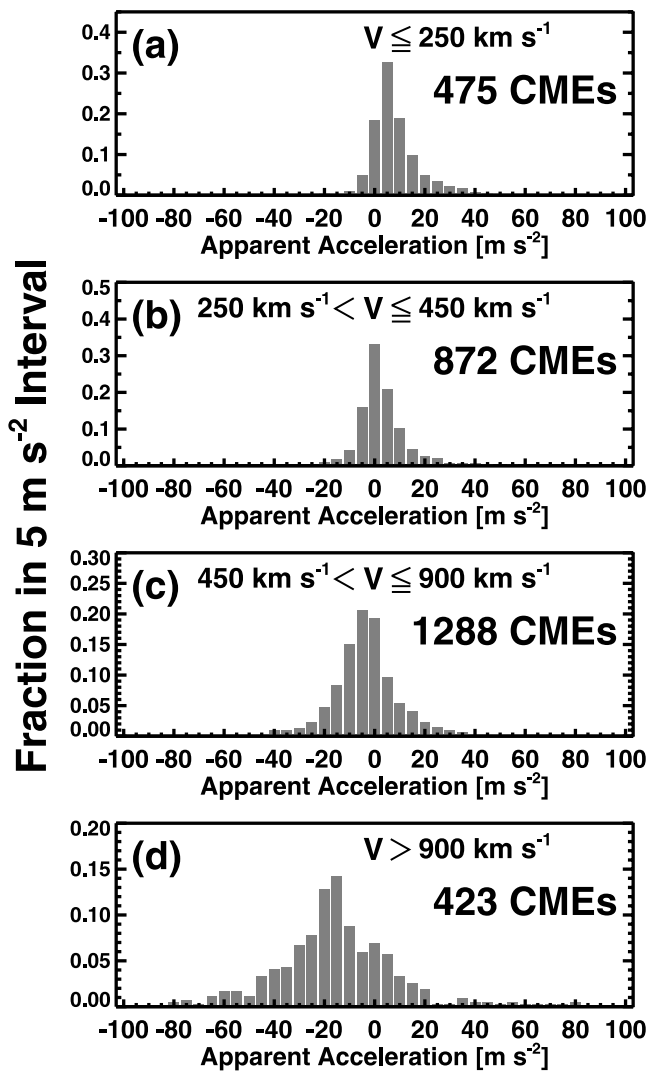


**Figure 8.** Acceleration distribution of the CMEs for various speed ranges. The fractions in  $5 \text{ m s}^{-2}$  interval are obtained by dividing the number of CMEs in each bin by the total number of CMEs.

and found that 23 CMEs listed in the work of *St. Cyr et al.* [2000] were not listed in our catalog, while 265 CMEs in our catalog were not listed in the work of *St. Cyr et al.* [2000]. We discuss the reasons for the discrepancy between *St. Cyr et al.* and our CME identifications.

[26] The main reason was different criteria for what constitutes a CME. If a new enhancement is detected in the coronagraph field of view but its outward motion is not clearly observed, the enhancement is called “coronal anomaly” [*St. Cyr et al.*, 2000]. In some cases, strong brightness enhancements were detected in streamers, but outward motion could be seen in only a few frames. *St. Cyr et al.* [2000] classified these as coronal anomalies, not CMEs, whereas we counted them as CMEs. Out of the 265 disputed CMEs, 110 were such anomaly events. Note that we can easily eliminate these anomaly events by selection of maximum height, since they faded quickly into the background in the C2 field of view.

[27] Another reason is the ability to separate CMEs that originate successively from the same general region. Eighty-six of the 265 CMEs belong to this category. For example, homologous jet-like CMEs frequently occurred at the same position angle for more than 1 day. *St. Cyr et al.* [2000] counted only the first one and made a comment “several more jets/tongue” in their list, but we counted all jet-like CMEs if they were clearly different from the remnants of the previous ones. We have also tried to identify new CMEs even if their leading edges had an overlap with the aftermath of a previous CME. The new CME is distinguished from the remnant of a previous CME by two aspects, shape and speed. Usually, the speed of the internal structure is the same or slightly less than the speed of the leading edge. If a faster structure follows, it has to be a different CME.

[28] One minor reason for the discrepancy was due to LASCO data gaps. *St. Cyr et al.* [2000] dropped seven CMEs owing to data gap and made a note of data gaps, but we counted these and measured them as CMEs. In addition, *St. Cyr et al.* did not include CMEs with angular width less than 5 but we have 10 such very narrow CMEs. However, our CME catalog does not have all polar microjets. Almost all 27 polar microjets reported by *Wang et al.* [1998] are not listed in the catalog (a few bright polar microjets are listed as CMEs).

[29] Therefore 215 out of the 265 events can be attributed to the different criteria employed in identifying CMEs. For the rest of the 50 events, we could not clarify the reason of the discrepancy. Similarly, it is not clear why the 23 events listed in the work of *St. Cyr et al.* [2000] are not in our list. Most likely, these are too faint and hence missed by the observer. However, we expect CME identification to vary, since manual measurements are subjective. Note that the disagreement of our CME identifications was only 7%.

#### 4.2. CME Trajectory

[30] The resultant acceleration depends on the propelling force (which drives the CME away from the Sun) and the retarding forces (gravity and drag). The measured acceleration therefore will have varying contributions from these forces. In section 3.4 we examined the CME acceleration/deceleration in several speed ranges. We found that most of the slow CMEs ( $V \leq 250 \text{ km s}^{-1}$ ) show acceleration, intermediate speed CMEs ( $250 < V \leq 450 \text{ km s}^{-1}$ ) have little acceleration, and most of the fast CMEs ( $V > 450 \text{ km s}^{-1}$ ) show deceleration. These results suggest that an interaction between the CMEs and solar wind is the most important mechanism that determines CME trajectories in the LASCO C2 and C3 FOV. This can be seen from the fact that CME trajectories change from acceleration to deceleration when the CME speed exceeds 250–450  $\text{km s}^{-1}$ , typical range of the slow solar wind speed. The deceleration for the fast CMEs was previously reported by *Gopalswamy et al.* [2001a] when comparing the acceleration profiles of fast ( $>900 \text{ km s}^{-1}$ ) CMEs with those of CMEs associated with type II radio bursts. They also found that the deceleration was quadratic in velocity and hence concluded that the coronal drag was responsible for the deceleration. *Gopalswamy et al.* [2000, 2001b] examined the relation between CME launch speed and CME travel time to the

Earth and found a correlation between CME launch speeds and mean accelerations. Their result suggests that the interaction between CMEs and the solar wind is important for CME propagation models in the interplanetary medium. Our results support their idea.

[31] As described above, most of the fast CMEs show deceleration motion in the LASCO C2 and C3 FOV. Indeed, there is no observation of a CME that accelerates from less than  $1000 \text{ km s}^{-1}$  to  $2000 \text{ km s}^{-1}$  in the LASCO C2 and C3 FOV. These results suggest that most of the fast CMEs must have finished accelerating before they reached the LASCO C2 FOV ( $\sim 2 R_s$ ). Any successful CME model has to explain the rapid acceleration below  $2 R_s$ , and the dominant retardation in the range  $2\text{--}32 R_s$ . In other words, CME models need to recognize the importance of propelling forces at  $<2 R_s$  and retarding (drag) forces beyond  $2 R_s$ .

[32] We saw that the average speed of CMEs is in the range  $300\text{--}500 \text{ km s}^{-1}$  (close to the slow solar wind speed), but the CME speed varies widely by two orders of magnitude. The minimum speed of  $\sim 30 \text{ km s}^{-1}$  is subsonic while the maximum speed of  $\sim 2600 \text{ km s}^{-1}$  is a super-Alfvénic speed in the corona. It is known that the speeds of the CMEs associated with large flares are greater [Gosling *et al.*, 1976; MacQueen and Fisher, 1983]. Hundhausen [1997] reported a weak correlation between CME kinetic energy and flare X-ray intensity (correlation coefficient is 0.53). There are fast CMEs ( $V > 1000 \text{ km s}^{-1}$ ) associated with B class flares, while there are X class flares without CMEs. The flare-CME relation is very complex. We found that there is weak correlation between CME speed and width for the CME with  $W > 60^\circ$ . The average speeds of normal and halo CMEs are  $428 \text{ km s}^{-1}$  and  $957 \text{ km s}^{-1}$ , respectively. Michael *et al.* [2003] investigated asymmetric halo CMEs by using a cone angle model and estimated that the average real width of halo CMEs is around  $120^\circ$ , more than twice of normal CMEs ( $47^\circ\text{--}61^\circ$ ). Therefore the halo CMEs seem to be inherently fast and wide. Wider CMEs tend to have higher speed and are associated with large flares. The CME speed-width relation may have something to do with the complex flare-CME relation. More intensive study is needed before arriving at firm conclusions.

#### 4.3. Future Plan

[33] We plan to include listings of special populations of CMEs, such as a halo CME list, a fast CME list, and so on. Although nearly 7000 CMEs were detected since 1996, only a small fraction (1–2%) of these CMEs are geoeffective [Gopalswamy *et al.*, 2003d]. Halo CMEs, if Earth-directed, can be geoeffective, causing geomagnetic storms provided they contain southward directed magnetic fields [Webb *et al.*, 2000; Zhang *et al.*, 2003]. The combination of LASCO images with EUV images in the form of movies will be useful in identifying the Earth-directed halo CMEs. Fast CMEs are considered geoeffective, since the fast CMEs are well associated with solar energetic particle (SEP) events [Kahler, 2001; Gopalswamy *et al.*, 2002; Gopalswamy, 2003]. Indeed, fast CMEs are important to understand the acceleration mechanisms of CMEs since fast CMEs are the control sample, as we discussed in section 4.2. Therefore a CME

catalog of special populations will help many researchers not only to investigate the Sun-Earth connection (space weather) but also to understand the origin of the CMEs.

## 5. Summary

[34] We have described the SOHO/LASCO CME catalog maintained on the World Wide Web. The total number of CMEs is nearly 7000 up to the end of 2002. The catalog has been open to the public for more than 2 years. Some errors and missing entries were pointed out by catalog users. We carefully reexamined them and revised them when necessary. We believe that the catalog is almost complete and will not have major revisions. However, since the identification and the measurements are made manually, there may be omissions of some faint CMEs. This catalog contains gross attributes of CMEs, which is ideally suited for statistical studies. However, we urge that researchers refer to original data for more detailed measurements and investigations.

[35] Using the catalog, we obtained the statistical properties of CMEs as follows: (1) The angular width distribution has two populations, one narrow ( $W \leq 20^\circ$ ) and the other normal ( $W > 20^\circ$ ) CMEs. The clear bimodal distribution was found only in 1998–2000 (early phase of solar maximum). (2) The average width of normal CMEs ( $20^\circ < W \leq 120^\circ$ ) increases from  $47^\circ$  (1996; solar minimum) to  $61^\circ$  (1999; early phase of solar maximum) and then decreases to  $53^\circ$  (2002; late phase of solar maximum). (3) CMEs are ejected approximately around the equator region during solar minimum, while during solar maximum CMEs originated from all latitudes. (4) The average speed of CMEs increases from  $300 \text{ km s}^{-1}$  (solar minimum) to  $500 \text{ km s}^{-1}$  (solar maximum). (5) The average speed of halo CMEs ( $957 \text{ km s}^{-1}$ ) is more than twice that of normal CMEs ( $428 \text{ km s}^{-1}$ ). (6) The slow CMEs ( $V \leq 250 \text{ km s}^{-1}$ ) show acceleration and fast CMEs ( $V > 900 \text{ km s}^{-1}$ ) show deceleration, suggesting that an interaction between the CME and solar wind is the most important mechanism that determines CME trajectories at  $2\text{--}32 R_s$ . Some of these results were also reported by the Solwind and SMM coronagraphs. However, a large number of LASCO CME observations revealed solar cycle variation in CMEs much more clearly than previous studies.

[36] **Acknowledgments.** The SOHO/LASCO data used here are produced by a consortium of the Naval Research Laboratory (USA), Max-Planck-Institut fuer Aeronomie (Germany), Laboratoire d'Astronomie (France), and the University of Birmingham (UK). SOHO is a project of international cooperation between ESA and NASA. The authors would like to thank S. Nunes, A. Rosas, P. K. Manoharan, G. Stenborg, W. Lu, A. Lara, and G. Lawrence for useful comments. The authors also thank the referees for the comments that have improved this manuscript. The catalog is developed in cooperation with the Naval Research Laboratory and the Solar Data Analysis Center (SDAC) at the NASA Goddard Space Flight Center. One of us (G. M.) was partly supported by Komitet Badań Naukowych through the grant PBZ-KBN-054/P03/2001. Part of this effort was also supported by the Air Force Office of Scientific Research (AFOSR), NASA/LWS, and NSF/SHINE (ATM 0204588).

[37] Shadia Rifai Habbal thanks Louise K. Harra, Bernard V. Jackson, and another referee for their assistance in evaluating this paper.

## References

- Brueckner, G. E., *et al.* (1995), The Large Angle Spectroscopic Coronagraph (LASCO), *Sol. Phys.*, *162*, 357–402.
- Burkepile, J. T., and O. C. St. Cyr (1993), A revised and expanded catalogue of coronal mass ejections observed by the Solar Maximum Mission coro-

- nagraph, *Tech. Note TN-369+STR*, Natl. Cent. for Atmos. Res., Boulder, Colo.
- Delaboudiniere, J.-P., et al. (1995), EIT: Extreme-Ultraviolet Imaging Telescope for the SOHO Mission, *Sol. Phys.*, *162*, 291–312.
- Domingo, V., B. Fleck, and A. I. Poland (1995), The SOHO mission: An overview, *Sol. Phys.*, *162*, 1–37.
- Fisher, R. R., R. H. Lee, R. M. MacQueen, and A. I. Poland (1981), New Mauna Loa coronagraph systems, *Appl. Opt.*, *20*, 1094–1101.
- Freeland, S. L., and B. N. Handy (1998), Data analysis with the SolarSoft system, *Sol. Phys.*, *182*, 497–500.
- Gopalswamy, N. (2003), Solar and geospace connections of energetic particle events, *Geophys. Res. Lett.*, *30*(11), 8013, doi:10.1029/2003GL017277.
- Gopalswamy, N., A. Lara, R. P. Lepping, M. L. Kaiser, D. Berdichevsky, and O. C. St. Cyr (2000), Interplanetary acceleration of coronal mass ejections, *Geophys. Res. Lett.*, *27*, 145–148.
- Gopalswamy, N., S. Yashiro, M. L. Kaiser, R. A. Howard, and J.-L. Bougeret (2001a), Characteristics of coronal mass ejections associated with long wavelength type II radio bursts, *J. Geophys. Res.*, *106*, 29,219–29,230.
- Gopalswamy, N., A. Lara, S. Yashiro, M. L. Kaiser, and R. A. Howard (2001b), Predicting the 1-AU arrival times of coronal mass ejections, *J. Geophys. Res.*, *106*, 29,207–29,218.
- Gopalswamy, N., S. Yashiro, G. Michalek, M. L. Kaiser, R. A. Howard, D. V. Reames, R. Leske, and T. von Roseninge (2002), Interacting coronal mass ejections and solar energetic particles, *Astrophys. J.*, *572*, L103–L107.
- Gopalswamy, N., A. Lara, S. Yashiro, and R. A. Howard (2003a), Coronal mass ejections and solar polarity reversal, *Astrophys. J.*, *598*, L63–L66.
- Gopalswamy, N., A. Lara, S. Yashiro, S. Nunes, and R. A. Howard (2003b), Coronal mass ejection activity during solar cycle 23, in *Solar Variability as an Input to the Earth's Environment, ESA SP-535*, edited by A. Wilson, pp. 403–414, Eur. Space Agency, Paris.
- Gopalswamy, N., M. Shimojo, W. Lu, S. Yashiro, K. Shibasaki, and R. A. Howard (2003c), Prominence eruptions and coronal mass ejection: A statistical study using microwave observations, *Astrophys. J.*, *586*, 562–578.
- Gopalswamy, N., S. Yashiro, A. Lara, M. L. Kaiser, B. J. Thompson, P. T. Gallagher, and R. A. Howard (2003d), Large solar energetic particle events of cycle 23: A global view, *Geophys. Res. Lett.*, *30*(10), 8015, doi:10.1029/2002GL016435.
- Gopalswamy, N., S. Nunes, S. Yashiro, and R. A. Howard (2004), Variability of solar eruptions during cycle 23, *Adv. Space Res.*, in press.
- Gosling, J. T., E. Hildner, R. M. MacQueen, R. H. Munro, A. I. Poland, and C. L. Ross (1976), The speeds of coronal mass ejection events, *Sol. Phys.*, *48*, 389–397.
- Hildner, E., J. T. Gosling, R. M. MacQueen, R. H. Munro, A. I. Poland, and C. L. Ross (1976), Frequency of coronal transients and solar activity, *Sol. Phys.*, *48*, 127–135.
- Howard, R. A., D. J. Michels, N. R. Sheeley Jr., and M. J. Koomen (1982), The observation of a coronal transient directed at earth, *Astrophys. J.*, *263*, L101–L104.
- Howard, R. A., N. R. Sheeley Jr., D. J. Michels, and M. J. Koomen (1985), Coronal mass ejections—1979–1981, *J. Geophys. Res.*, *90*, 8173–8191.
- Howard, R. A., et al. (1997), Observations of CMEs from SOHO/LASCO, in *Physics of the Magnetopause, Geophys. Monogr. Ser.*, vol. 99, edited by P. Song, B. U. Ö. Sonnerup, and M. F. Thomsen, pp. 17–26, AGU, Washington, D.C.
- Hundhausen, A. J. (1993), Sizes and locations of coronal mass ejections—SMM observations from 1980 and 1984–1989, *J. Geophys. Res.*, *98*, 113–177.
- Hundhausen, A. J. (1997), An introduction, in *Coronal Mass Ejections, Geophys. Monogr. Ser.*, vol. 99, edited by N. Crooker, J. Joselyn, and J. Feynman, pp. 1–7, AGU, Washington, D.C.
- Hundhausen, A. J., C. B. Sawyer, L. House, R. M. E. Illing, and W. J. Wagner (1984), Coronal mass ejections observed during the solar maximum mission—Latitude distribution and rate of occurrence, *J. Geophys. Res.*, *89*, 2639–2646.
- Hundhausen, A. J., J. T. Burkepile, and O. C. St. Cyr (1994), Speeds of coronal mass ejections: SMM observations from 1980 and 1984–1989, *J. Geophys. Res.*, *99*, 6543.
- Kahler, S. W. (1992), Solar flares and coronal mass ejections, *Annu. Rev. Astron. Astrophys.*, *30*, 113.
- Kahler, S. W. (2001), The correlation between solar energetic particle peak intensities and speeds of coronal mass ejections: Effects of ambient particle intensities and energy spectra, *J. Geophys. Res.*, *106*, 20,947–20,955.
- MacQueen, R. M., and R. R. Fisher (1983), The kinematics of solar inner coronal transients, *Sol. Phys.*, *89*, 89–102.
- MacQueen, R. M., J. A. Eddy, J. T. Gosling, E. Hildner, R. H. Munro, G. A. Newkirk, A. I. Poland, and C. L. Ross (1974), The outer solar corona as observed from Skylab: Preliminary results, *Astrophys. J.*, *187*, L85–L88.
- MacQueen, R. M., A. Csoeke-Poeckh, E. Hildner, L. House, R. Reynolds, A. Stanger, H. Tepoel, and W. Wagner (1980), The High Altitude Observatory Coronagraph/Polarimeter on the Solar Maximum mission, *Sol. Phys.*, *65*, 91–107.
- Michalek, G., N. Gopalswamy, and S. Yashiro (2003), A new method for estimating widths, velocities, and source location of halo coronal mass ejections, *Astrophys. J.*, *584*, 472–478.
- Michels, D. J., R. A. Howard, M. J. Koomen, and N. R. Sheeley Jr. (1980), Satellite observations of the outer corona near sunspot maximum, in *Radio Physics of the Sun*, edited by M. R. Kundu and T. E. Gergely, pp. 439–442, D. Reidel, Norwell, Mass.
- Sheeley, N. R., Jr., et al. (1997), Measurements of flow speeds in the corona between 2 and 30  $R_{\odot}$ , *Astrophys. J.*, *484*, 472.
- Sheeley, N. R., Jr., W. N. Hakala, and Y.-M. Wang (2000), Detection of coronal mass ejection associated shock waves in the outer corona, *J. Geophys. Res.*, *105*, 5081–5092.
- St. Cyr, O. C., and J. T. Burkepile (1990), A catalogue of mass ejections observed by the solar maximum mission coronagraph, *Tech. Note NCAR/TN-352+STR*, Natl. Cent. for Atmos. Res., Boulder, Colo.
- St. Cyr, C. O., J. T. Burkepile, A. J. Hundhausen, and A. R. Lecinski (1999), A comparison of ground-based and spacecraft observations of coronal mass ejections from 1980–1989, *J. Geophys. Res.*, *104*, 12,493–12,506.
- St. Cyr, O. C., et al. (2000), Properties of coronal mass ejections: SOHO LASCO observations from January 1996 to June 1998, *J. Geophys. Res.*, *105*, 18,169–18,185.
- Tousey, R. (1973), The solar corona, in *Space Research XIII*, edited by M. J. Rycroft and S. K. Runcorn, pp. 713, Akademie-Verlag, Berlin.
- Tousey, R., R. A. Howard, and M. J. Koomen (1974), The frequency and nature of coronal transient events observed by OSO-7, *Bull. Am. Astron. Soc.*, *6*, 295.
- Wang, Y.-M., et al. (1998), Observations of correlated white-light and extreme-ultraviolet jets from polar coronal holes, *Astrophys. J.*, *508*, 899–907.
- Webb, D. F., E. W. Cliver, N. U. Crooker, O. C. St. Cyr, and B. J. Thompson (2000), Relationship of halo coronal mass ejections, magnetic clouds, and magnetic storms, *J. Geophys. Res.*, *105*, 7491–7508.
- Zhang, J., K. P. Dere, R. A. Howard, and V. Bothmer (2003), Identification of solar sources of major geomagnetic storms between 1996 and 2000, *Astrophys. J.*, *582*, 520–533.

N. Gopalswamy, O. C. St. Cyr, and S. Yashiro, NASA Goddard Space Flight Center, Code 695.0, Greenbelt, MD 20771, USA. (gopals@fugee.gsfc.nasa.gov; chris.stcyr@nasa.gov; yashiro@cdaw.gsfc.nasa.gov)

R. A. Howard, S. P. Plunkett, and N. B. Rich, Solar Physics Branch, Space Sciences Division, Naval Research Laboratory, Washington, DC 20375, USA. (russ.howard@nrl.navy.mil; simon.plunkett@nrl.navy.mil; nathan.rich@nrl.navy.mil)

G. Michalek, Astronomical Observatory of Jagiellonian University, ul. Orla 171, Krakow 30-244, Poland. (michalek@oa.uj.edu.pl)